







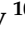
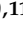



Article

Polyol Synthesis of Ag-Doped Copper Oxide Nanoparticles as a Methylene Blue-Degrading Agent

Yogeshwar Baste ¹, Vikram Jadhav ², Arpita Roy ^{3,*}, Saad Alghamdi ⁴, Mohamed Abbas ⁵,
Jari S. Algethami ^{6,7}, Mazen Almeahmadi ⁸, Mamdouh Allahyani ⁸, Devvret Verma ⁹,
Krishna Kumar Yadav ^{10,11}, Byong-Hun Jeon ^{12,*} and Hyun-Kyung Park ¹³

- ¹ Department of Chemistry, K.S.K.W Arts, Science & Commerce College, Cidco, Uttam Nagar, Nashik 422008, Maharashtra, India; yogeshwarbaste@yahoo.co.in
- ² Department of Chemistry, M.V.P. Samaj's K.K. Wagh Arts, Science, and Commerce College, Pimpalgaon (B.), Nashik 422209, Maharashtra, India; mevikramjadhav@gmail.com
- ³ Department of Biotechnology, Sharda School of Engineering & Technology, Sharda University, Greater Noida 201310, Uttar Pradesh, India
- ⁴ Laboratory Medicine Department, Faculty of Applied Medical Sciences, Umm Al-Qura University, Makkah 21955, Saudi Arabia; ssalghamdi@uqu.edu.sa
- ⁵ Electrical Engineering Department, College of Engineering, King Khalid University, Abha 61421, Saudi Arabia; mabas@kku.edu.sa
- ⁶ Department of Chemistry, College of Science and Arts, Najran University, Najran 11001, Saudi Arabia; jsalgethami@nu.edu.sa
- ⁷ Promising Centre for Sensors and Electronic Devices (PCSED), Najran University, Najran 11001, Saudi Arabia
- ⁸ Department of Clinical Laboratory Sciences, College of Applied Medical Sciences, Taif University, P.O. Box 11099, Taif 21944, Saudi Arabia; mazenn@tu.edu.sa (M.A.); m.allahyani@tu.edu.sa (M.A.)
- ⁹ Department of Biotechnology, Graphic Era Deemed to be University, Dehradun 248002, Uttarakhand, India; devvret@gmail.com
- ¹⁰ Faculty of Science and Technology, Madhyanchal Professional University, Bhopal 462044, Madhya Pradesh, India; envirokrishna@gmail.com
- ¹¹ Environmental and Atmospheric Sciences Research Group, Scientific Research Center, Al-Ayen University, Thi-Qar, Nasiriyah 64001, Iraq
- ¹² Department of Earth Resources and Environmental Engineering, Hanyang University, 222 Wangsimni-ro, Seongdong-gu, Seoul 04763, Republic of Korea
- ¹³ Department of Pediatrics, Hanyang University College of Medicine, 222 Wangsimni-ro, Seongdong-gu, Seoul 04763, Republic of Korea; neopark@hanyang.ac.kr
- * Correspondence: arbt2014@gmail.com (A.R.); bhjeon@hanyang.ac.kr (B.-H.J.)



Citation: Baste, Y.; Jadhav, V.; Roy, A.; Alghamdi, S.; Abbas, M.; Algethami, J.S.; Almeahmadi, M.; Allahyani, M.; Verma, D.; Yadav, K.K.; et al. Polyol Synthesis of Ag-Doped Copper Oxide Nanoparticles as a Methylene Blue-Degrading Agent. *Catalysts* **2023**, *13*, 1143. <https://doi.org/10.3390/catal13071143>

Academic Editors: Magdalena Janus and Carl Redshaw

Received: 19 June 2023

Revised: 19 July 2023

Accepted: 19 July 2023

Published: 23 July 2023



Copyright: © 2023 by the authors. Licensee MDPI, Basel, Switzerland. This article is an open access article distributed under the terms and conditions of the Creative Commons Attribution (CC BY) license (<https://creativecommons.org/licenses/by/4.0/>).

Abstract: The use of metal oxide nanomaterials as photocatalysts for wastewater treatment has received significant attention in recent years due to their unique physicochemical properties. In this study, we use a polyol-mediated refluxing method to synthesize silver-incorporated copper oxide nanomaterials (Ag@CuO NMs). The use of tetra butyl ammonium bromide (TBAB) as a capping agent and ethylene glycol as a reducing agent for Ag⁺ to Ag is elaborated upon. The prepared Ag@CuO NMs were tested for their ability to degrade water pollutants, specifically methylene blue (MB) dye. Two different Ag contents, weights of 3% and 5%, were used to produce modified CuO-based nanomaterials. The crystalline structures of the NMs were characterized via XRD diffraction, and the morphology of the materials was investigated using FE-SEM. The optical properties were studied using UV-vis spectroscopy. The photocatalytic activity of the Ag@CuO NMs was evaluated by analyzing the degradation of MB dye when exposed to UV-visible light. Our results showed that the 5% weight Ag@CuO NM sample exhibited the most efficient degradation activity against MB dye. Therefore, these nanomaterials hold potential for photocatalytic applications, particularly for wastewater purification.

Keywords: methylene blue; photocatalytic activity; refluxing method; Ag@CuO Ns

1. Introduction

Environmental pollution is an issue that affects both developed and developing nations alike, and it stems from a variety of sources, including the overuse of natural resources, synthetic organic products, inadequate regulations, and a lack of environmental awareness [1]. While several scientific studies have focused on developing novel synthesis methods and adopting eco-friendly practices in recent years [2], industrial processes still generate various goods, by-products, and other materials using inputs such as raw materials, water, light, and energy [3]. However, the types and quantities of dye waste produced during different phases of human activities can vary based on production techniques and consumption trends [4]. Those worried about the outcomes share concerns about the environment and human health. Freshwater plays an essential role in living things everywhere. Water covers over 70% of the Earth, yet only a relatively small percentage, about 2.5%, is used for various uses, including human activities. The industrial revolution spread throughout the whole world due to uncontrolled population expansion, which contaminated land, air, and water bodies, particularly with industrial pollutants that are highly hazardous and non-biodegradable. Most textile companies consume much more water throughout the dyeing, cleaning, and other processes. About 60% of the colors used in the production of industrial textile products are combined with wastewater [5,6].

One of the primary sources of pollution is the spread of this contaminated wastewater throughout the environment. Poisonous species discharged through non-fabricating actions, such as deadwood, contagions, harmful microbes, germ-free crops, and cleaner trash, are included in residential wastewater [7–9]. A significant contributor to water contamination is the presence of this pollutant in untreated water. According to the literature survey of researchers' investigations, several management organizations have employed various recycling plans for polluted water that are physically, physiologically, and chemically similar to those found in nature [8,10]. Photocatalysis is the most excellent method for purifying water among the several treatment options. It involves the absorption of light energy to form e^-/h^+ pairs, which subsequently produce redox chemical processes on the surface of the photocatalyst material; these processes take place simultaneously [11]. In recent years, there has been a view of the development of photocatalysis as a flexible process with several uses, such as the auto-sterilization and cleaning of glassware, H_2O splitting, organic contamination oxidation, and the degradation of crude materials and aromatic or nonaromatic hydrocarbons [12]. Depending on the phase condition of the constituents, the photocatalytic process is divided into two types: homogeneous (when both the substrate and photocatalyst are in the same phase) and heterogeneous (when both the substrate and photocatalyst are in different stages) photocatalysis. Artificially prepared $TiO_{2(s)}$ is the most investigated photocatalyst among the many explored semiconducting nanomaterials [13]. Numerous efforts have been made to improve the photocatalytic performance of $TiO_{2(s)}$ and other metal oxides, including the use of various production processes, transition metal doping, non-metal doping, anion/cation doping, linked catalysts, and noble metal doping/composites [14]. Advanced reaction approaches include the photocatalytic treatment or action of chemical contaminants employing semiconductors as photocatalysts. Research on semiconductors such as $TiO_{2(s)}$ photocatalytic activity has been published [15,16]. $TiO_{2(s)}$ and most other photocatalysts are barely responsive to UV irradiation, which consumes 4% of solar energy, severely restricting their wide-ranging practical use. $TiO_{2(s)}$ usage is greatly hampered since direct sunlight generally comprises just 4% of UV light, compared to visible light's 43% of limitless solar energy [17].

Several metal/metal oxides, including $Au_{(s)}$, $Ag_{(s)}$, $Pt_{(s)}$, $CaO_{(s)}$, $ZnO_{(s)}$, $NiO_{(s)}$, $Ag_2O_{(s)}$, $TiO_{2(s)}$, $CuO_{(s)}$, were used in photocatalysis to purify wastewater [18–21]. $CuO_{(s)}$ stands out from the rest due to its availability, inexpensive, non-hazardous, and stable nature when exposed to light, which has led to its widespread application in photocatalysis. $CuO_{(s)}$ has a monoclinic crystal system, and copper (Cu) shows variable oxidation states, including Cu^+ , Cu^{2+} , and Cu^{3+} , making it equally attractive for doping with h^+ and e^- pairs. $CuO_{(s)}$ is used in biomedicine as a photocatalytic agent, anticancer agent, drug delivery agent, and

mediator. $\text{CuO}_{(s)}$ is also widely used as a p-type semiconductor in industrial applications such as wireless communications, gas sensors, and solar technology. $\text{CuO}_{(s)}$ has previously been doped with several elements to increase its photodegradation activity [22,23]. For instance, El Sayed, A. M., and Shaban, M. Shaban looked into the effect of Fe– $\text{CuO}_{(s)}$ and discovered more excellent activity due to Fe doping [24]. Mo– $\text{CuO}_{(s)}$ nanostructures were created by Maraj M. et al., who then assessed their photocatalytic activity against dyes [25].

Similarly, Devi et al. improved $\text{CuO}_{(s)}$ photocatalytic dye degradation activity by incorporating it with Tb [26]. These monoclinic Tb-doped $\text{CuO}_{(s)}$ nanoparticles were made using a combustion technique. The increased surface area significantly improved the degrading activity against various dyes. When exposed to UV-Vis radiation, the valence-band (VB) electrons immediately become promoted and moved towards the conduction band (CB). $\text{CuO}_{(s)}$ is a p-type semiconductor with a 3.37 eV and 60 MeV direct band gap and exciting binding energy (BE), respectively, due to the VB empty sites producing electron–hole pairs as a consequence [27]. As a result, electrons collect in the CB, whereas holes accumulate in the VB. These holes in the band's valence create hydroxyl groups when they interact with water molecules, which then combine with the dye to produce the degradation products, along with carbon dioxide and water. Oxygen reduction to $\text{O}_{2(g)}$ due to an interaction between oxygen atoms and conduction band electrons can also cause deterioration [28,29].

In this work, we have synthesized polyol-mediated Ag– CuO NPs using a refluxing method in which the silver nitrate contents of 3 and 5 wt.% were used. The 5 wt.% silver nitrates in polyol-mediated the Ag– CuO NP material showed enhanced optical and photocatalytic properties due to a higher percentage of Ag doping [30,31].

2. Results and Discussion

2.1. UV-Vis Absorption Spectroscopy Analysis

The absorption spectra of polyol-mediated Ag@ CuO nanomaterial, shown in Figure 1, exhibit an absorption peak at 214 nm. This absorption peak corresponds to the significant exciton binding energy of Ag@ $\text{CuO}_{(s)}$ at room temperature. The size of the nanomaterial influences the band gap until the synthesis time, resulting in a slight shift. The optical absorption edge of Ag@ $\text{CuO}_{(s)}$ undergoes a marginal change towards a longer wavelength as the annealing synthesis time reaches 3 h. This change can be associated with the growth in grain size. UV-Vis analysis indicates that the band gap shift from its standard value, caused by the size impact on Ag@ $\text{CuO}_{(s)}$ crystallinity, is more pronounced than that of the bulk material (1.72 eV) due to the synthesis time. This finding suggests that the nanomaterial exhibits significant absorption capacity within the region [26,28].

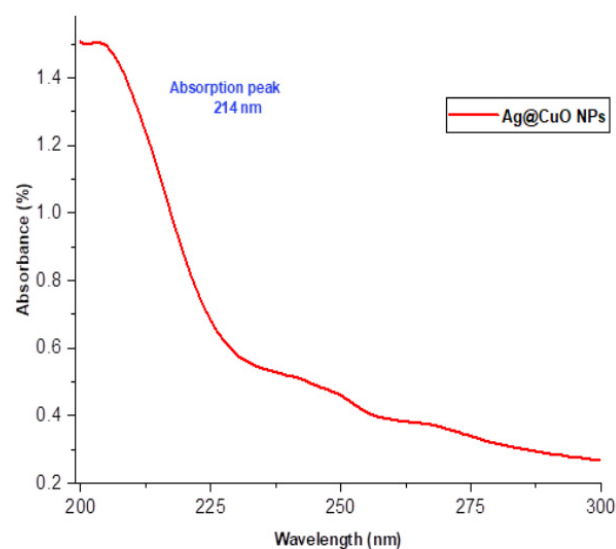


Figure 1. UV-Vis spectra of polyol-mediated Ag@ CuO NMs.

2.2. FT-IR Analysis

FTIR analysis was conducted to gain insight into the chemical and structural characteristics of the synthesized polyol-mediated Ag@CuO NPs and the effect of the substances on the nanomaterials. Figures 2 and 3 display the polyol-mediated Ag@CuO material before and after calcination, respectively, and the spectrum was recorded from 400 to 4000 cm^{-1} . In Figure 2, two prominent bands, the Au and Bu modes, were observed at 497 cm^{-1} and 606 cm^{-1} , respectively. The Au mode refers to a specific vibrational mode involving atomic motion within the material, typically associated with a particular arrangement or coordination of atoms. Without further information about the specific compound or material being studied, the frequency of 497 cm^{-1} suggests a specific type of bonding or structural feature within the material. Similarly, the Bu mode observed at 606 cm^{-1} represents another distinct vibrational mode associated with the material. Again, without additional context, it is challenging to pinpoint the exact nature of the Bu mode. The frequency of 606 cm^{-1} indicates a specific molecular vibration or interaction present in the sample. The band at 1649 cm^{-1} was assigned to C-N and C-C stretching, indicating the presence of amine groups, and the band at 1470 cm^{-1} was for the N-H stretch vibration present in the molecules. The peak at 497 cm^{-1} was attributed to the Cu-O stretching vibration mode, while the high-frequency mode at 606 cm^{-1} was associated with the Cu-O stretching mode. No other IR active mode was observed in the 607 to 660 cm^{-1} region, ruling out the presence of another phase, such as Cu_2O . The presence of small peaks observed at 1374 cm^{-1} in the FTIR spectra of the nanocomposites indicates the presence of silver nanoparticles. In FTIR spectroscopy, peaks are produced via the absorption of infrared light by specific chemical bonds within a sample. Each peak corresponds to a specific vibrational mode of the bonds present in the material. In the case of the nanocomposites, the observed peak at 1374 cm^{-1} suggests the presence of bonds involving silver atoms. Without additional information about the specific experimental conditions or the exact composition of the nanocomposites, it is difficult to provide a definitive explanation for the exact nature of the silver bonds responsible for this peak.

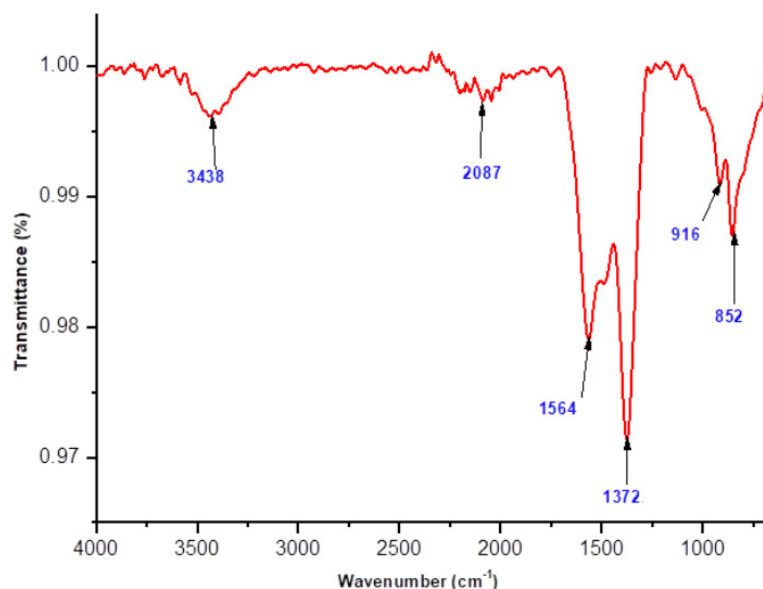


Figure 2. FTIR spectrum of polyol-mediated compound before calcination.

However, in general, silver nanoparticles can exhibit characteristic vibrational modes in the infrared region due to their unique structure and bonding. The peak at 1374 cm^{-1} could arise from vibrations associated with the chemical bonds between silver atoms or between silver and other atoms present in the nanocomposites. These bonds may involve silver–oxygen (Ag–O) or silver–carbon (Ag–C) interactions, among others. To reach a more precise understanding of the origin of the observed peaks, further analysis and

characterization techniques, such as X-ray diffraction (XRD) or electron microscopy, may be necessary. These techniques can provide complementary information about the crystal structure, morphology, and elemental composition of the nanocomposites, helping to confirm the presence and specific bonding environment of the silver nanoparticles.

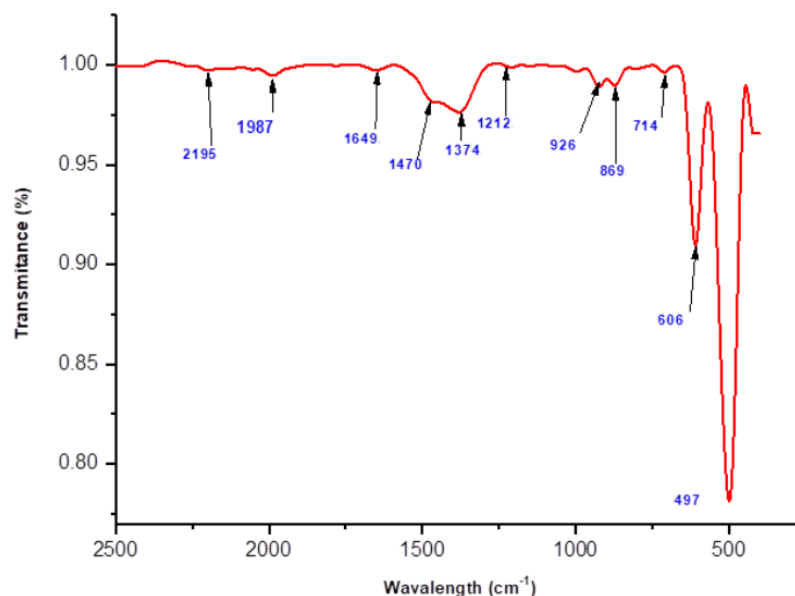


Figure 3. FTIR spectrum of polyol-mediated Ag@CuO NPs (after calcination).

2.3. X-ray Diffraction Microscopy (XRD)

The crystalline structure of synthesized Ag@CuO NPs was studied using X-ray diffraction (XRD), as shown in Figure 4. The XRD pattern confirms the formation of a monoclinic phase during the use of the refluxing method. The diffraction peaks observed at 2θ values of 32.41° , 35.52° , 38.66° , 48.89° , 53.39° , 58.12° , 61.62° , and 68.06° correspond to the crystal planes (110), (111), (200), (-202), (020), (202), (-113), and (022) of CuO, respectively. Additional peaks at 38.60° , 44.28° , 64.50° , and 77.32° correspond to the crystal planes (111), (220), (220), and (311) of Ag. The perfect match between all the diffraction peaks and the monoclinic CuO (JCPDS no. 80-1917) and cubic Ag (JCPDS no. 04-0783) confirms that the nanomaterials are entirely made of Ag@CuO [30–32].

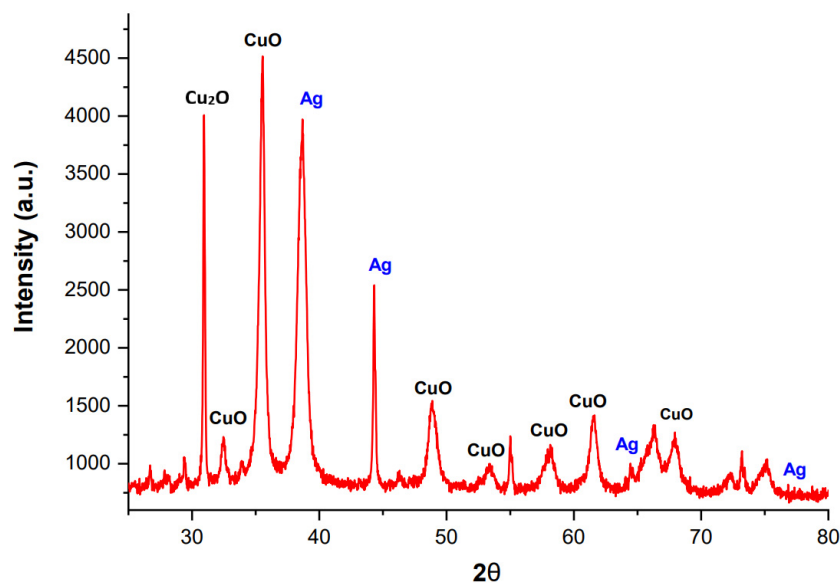


Figure 4. XRD pattern of polyol-mediated Ag@CuO NPs.

The calculation of d spacing (Ag@CuO NPs) is carried out as follows:
Bragg's equation is

$$n\lambda = 2d \sin \theta$$

where

$\lambda = 1.54 \text{ \AA}$ (wavelength of X rays),

$n =$ order of diffraction ($n = 1$),

$d =$ distance between adjacent NPs layers,

$\theta =$ diffraction angle

The d spacing equation is as follows:

$$d = \frac{n \lambda}{2 \times \sin \theta}$$

The equation for crystal planes of the monoclinic system is as follows:

$$d_{hkl} = \sqrt{\frac{a^2}{h^2} + \frac{b^2}{k^2} + \frac{c^2}{l^2}}$$

The lattice parameters are $a = 4.683 \text{ \AA}$, $b = 3.421 \text{ \AA}$ and $c = 5.129 \text{ \AA}$

The Scherrer equation for average crystalline size is as follows:

$$D = \frac{K \lambda}{\beta \cos \theta} \quad (D \leq 200 \text{ nm})$$

where $D =$ average particle size, $K =$ Scherrer constant, $\beta = \beta' \pi / 180$, broadening at FWHM in radians, and $\beta' =$ full width at half maximum.

Using the above Scherrer equation, the mean or average particle size of the polyol-mediated Ag@CuO NPs is 24.02 nm.

2.4. Field Emission Scanning Electron Microscopy (FE-SEM)

The FE-SEM analysis showed that the synthesized nanomaterials had gaps for smooth ion transport that were randomly distributed on their surface. After Ag doping, the substance was transformed into evenly dispersed nanoparticles, with an average particle size ranging between 60 and 120 nm (Figure 5). The particles were observed to be rod-shaped, spherical, and round with a group of aggregations. In contrast, XRD spectra revealed an average particle size of 24.02 nm. The FTIR analysis showed weak and strong bonding peaks of Ag, Cu, and O atoms due to organic molecules such as alcoholic and amine compounds and weak peaks due to C, N, Ag, Cu, and O. These synthesized nanoparticles had enhanced surface characteristics and the presence of active sites for the bonding and degradation of dye molecules.

The photocatalytic dye degradation mechanism is shown below.

Charge initiation process:

Photocatalytic dye degradation steps [1]

which are responsible for the photocatalytic activity of the material. The excited electrons (e^-) in the CB can participate in redox reactions with the adsorbed dye molecules, while the holes (h^+) in the VB can react with the hydroxyl ions (OH^-) to produce highly reactive hydroxyl radicals ($\bullet OH$) that can oxidize the dye molecules (Figure 6). The overall process results in the degradation of the dye molecules and the production of harmless products. Therefore, the Ag@CuO NPs can be used as efficient photocatalysts for degrading organic pollutants under visible light irradiation.

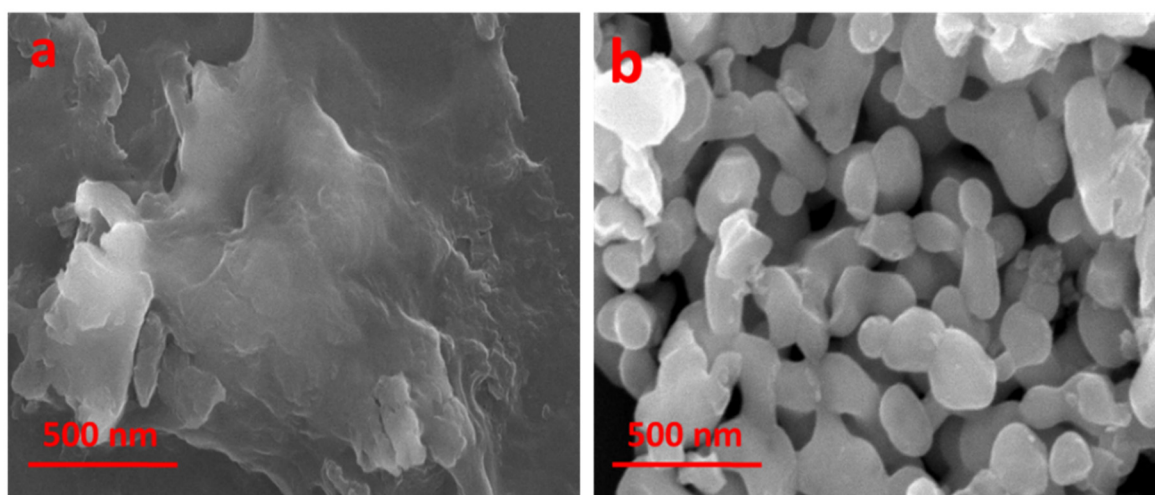


Figure 5. FE-SEM images of polyol-mediated Ag@CuO NPs (a) before calcination and (b) after calcination.

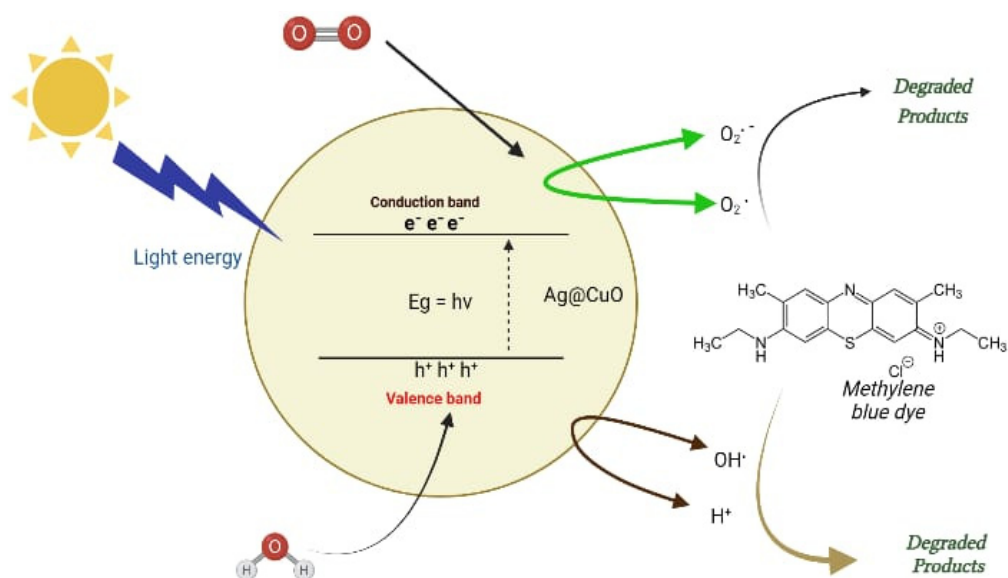
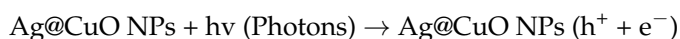
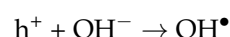
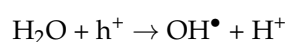


Figure 6. Photocatalytic dye degradation mechanism using Ag@CuO NPs.

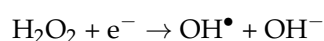
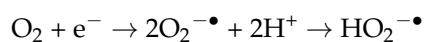


An electron is promoted to the CB, and its excitation leaves a h^+ in the valence band.
Charge carrier process: [33]

The hole (h^+) in the VB act as an oxidizing agent directly oxidized to dyes or combined with H_2O to produce HO^\bullet radicals.



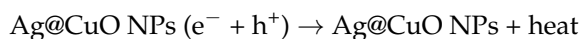
At another site, the electron in the CB reacts with another molecule such as O_2 and H_2O_2 to generate several reactive species such as $\text{O}_2^{\bullet-}$ and HO_2^\bullet , which is shown in the following steps.





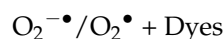
Charge carriers' recombination:

The heat evolved during the recombination of charge carriers ($e^- + h^+$).



Photocatalytic degradation of dyes: [34,35]

Photocatalytic dye degradation processes with the ($e^- + h^+$) pairs play the leading role, in which $\text{OH}^{-\bullet}$, O_2^{\bullet} , and HO_2^{\bullet} radicals and holes (h^+) are intermediates that react spontaneously on the neighboring ions, degrading the dye compounds. During the degradation process, the charge species such as OH^{\bullet} , h^+ , and e^- act as oxidizing and reducing agents.



The mechanism of photocatalytic dye degradation using Ag@CuO NPs is shown in Figure 7.

The mechanism of photocatalytic dye degradation using Ag@CuO nanoparticles involves the absorption of light, the generation of electron–hole pairs, redox reactions with dye molecules and reactive oxygen species (ROS), the adsorption of dye molecules onto the nanoparticles, electron transfer from nanoparticles to dye molecules leading to their reduction, hole oxidation generating highly reactive hydroxyl radicals, the formation of other reactive oxygen species, and the complete degradation of the dye into harmless byproducts. The specific details and kinetics can vary depending on various factors [36,37].

Experimental photo degradation procedure:

This experiment involved using 20 mg/mL of polyol-mediated Ag@CuO NPs, and the absorption spectra for the model pollutant, 0.20 mg/mL of methylene blue (MB), dye were measured. For the concentrations of Ag@CuO NPs, which are unique to MB, the spectra indicated a maximum wavelength of 660 nm. The Ag@CuO NPs were left in the dark for 10 min throughout the experiment to be observed, and the dye did not degrade. When Ag@CuO NPs were added to the same stock solution and subjected to visible light radiation, the absorption dramatically altered over 15 min. The absorption at 0 min was more significant for samples with a higher Ag@CuO NP content than for samples with a lower Ag@CuO concentration. This is because increased Ag@CuO NP concentrations will result in more molecules interacting with light waves, increasing absorption. For these samples, absorption decreased and was equivalent after 30 min. We continued to process for 120 min, recorded the absorption and observed the methylene blue dye degradation [33,34].

A higher concentration of Ag@CuO NPs (20 mg/100 mL) resulted in a remarkable degradation of 94.43% of dye, while the lower concentration of Ag@CuO (10 mg/100 mL) showed a lower percentage of dye degradation after 105 min. In this study, methylene blue dye underwent 50% degradation in 10 min in a 0.02 mg/mL concentration. When Ag@CuO NPs were added at a concentration of 0.3 mg/mL, the absorption rate decreased exponentially, as demonstrated in Figure 7B. The absorbance vs. wavelength plot in Figure 7A indicated a low degradation rate of methylene blue dye. The calculations presented in this study are solely based on the polyol-mediated Ag@CuO nanomaterial after calcination [34].

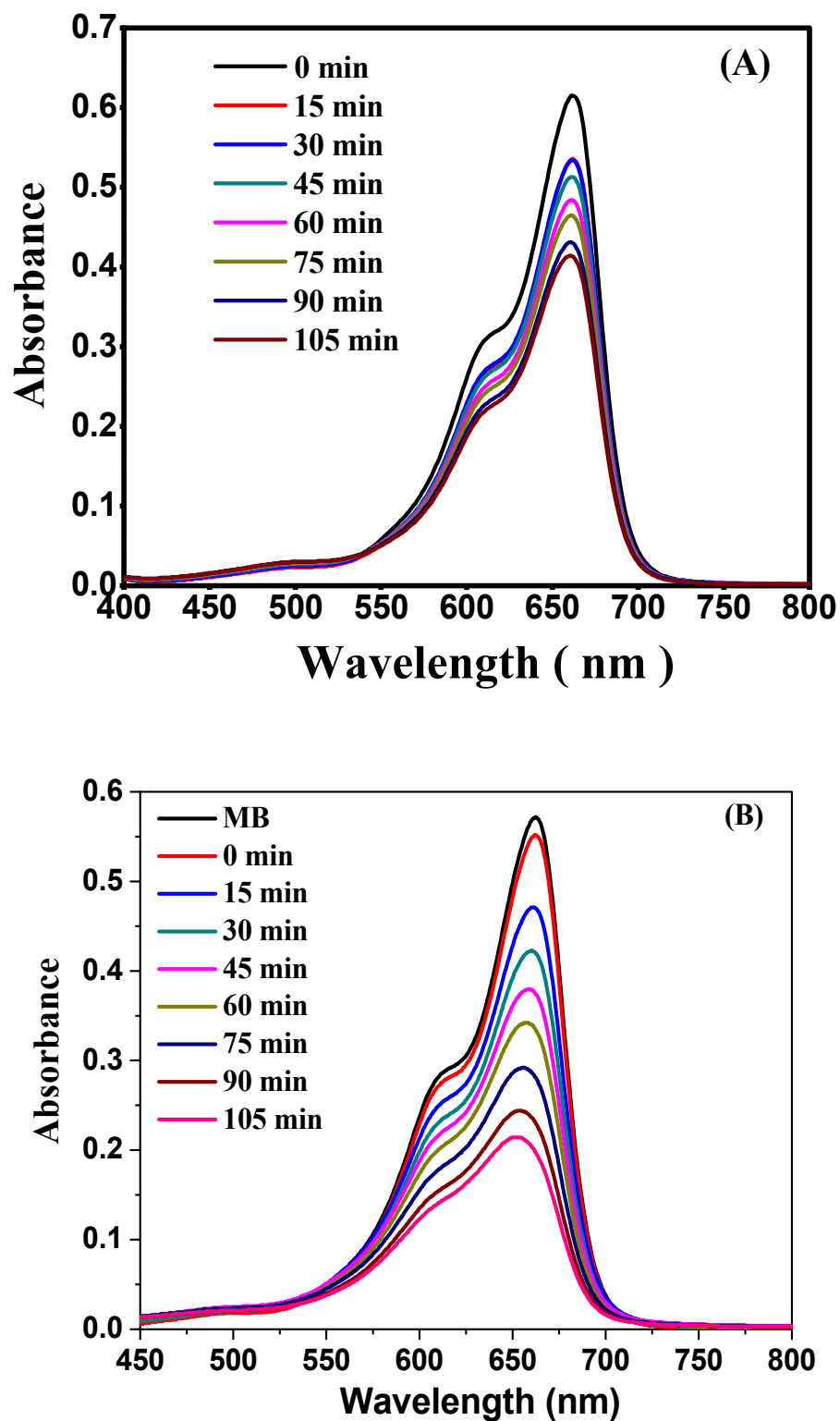


Figure 7. Absorbance vs. wavelength plot. (A) Dye degradation using material before calcination and (B) dye degradation using polyol-mediated Ag@CuO NPs (after calcination).

The percentage of degradation was calculated using

$$\text{Degradation (\%)} = \frac{C_0 - C}{C} \times 100$$

where, C_0 and C are the initial and final concentrations of MB at the time (t) ($C_0 = 0.5752$ and $C = 0.032$ ($t = 125$ min)).

$$\text{Degradation (\%)} = \frac{0.5752 - 0.032}{0.5752} \times 100$$

$$\text{Degradation (\%)} = 94.43\%$$

Methylene blue dye degradation obeys the 1st order chemical kinetics, the velocity constant (K) and half-life time ($t_{1/2}$) calculated using the following equations:

$$K = \frac{1}{t} \ln \frac{C_0}{C} \text{ and } t_{1/2} = \frac{0.693}{K}$$

Figure 8 shows the kinetics of methylene blue at a concentration of 0.20 mg/mL reacting with the added polyol-mediated Ag@CuO NPs reaction at a concentration of 20 mg/100 mL. The slope of the equation directly gives the rate constant. The rate constant is $8.641 \times 10^{-3} \text{ min}^{-1}$.

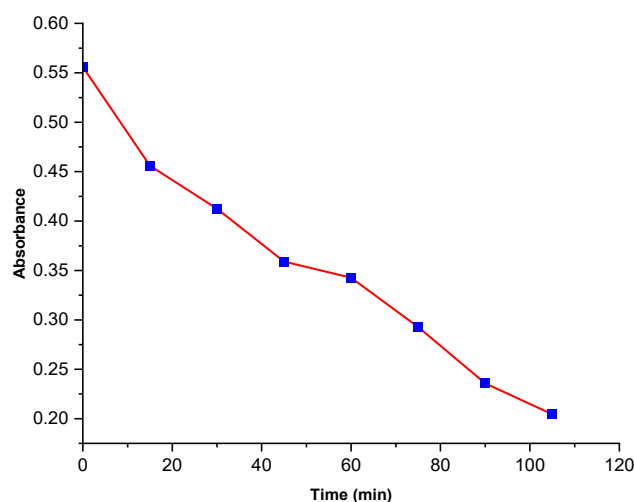


Figure 8. Absorbance vs. time of MB dye degradation.

The k was also determined from the linear plot of absorbance vs. time (t).

Based on the rate constant value of 8.641×10^{-3} obtained from the methylene blue dye degradation experiment using polyol-mediated Ag@CuO nanomaterial (Table 1), it may be suggested that the given reaction rate is relatively fast. This result is promising and could have potential implications on various industries, such as water treatment and wastewater management. However, further research and experimentation would be necessary to understand the extent and scope of its applications fully [36–38].

Table 1. Mean value of rate constant of the photocatalytic dye degradation.

Sr. No.	Time (min)	Absorbance (A) of MB	Rate Constant (K) min^{-1}	The Mean Value of Rate Constant (K) min^{-1}
1	0	0.5560	-	
2	15	0.4560	1.548×10^{-2}	
3	30	0.4125	1.108×10^{-2}	
4	45	0.3590	1.047×10^{-2}	
5	60	0.3426	8.635×10^{-3}	8.641×10^{-3}
6	75	0.2928	9.003×10^{-3}	
7	90	0.2359	9.903×10^{-3}	
8	105	0.2045	9.849×10^{-3}	

3. Materials and Methods

3.1. Materials

Copper acetate ($\text{Cu}(\text{CH}_3\text{COO})_2$) as a precursor, silver nitrate (AgNO_3) as a source of Ag, tetra butyl ammonium bromide (TBAB) ($\text{C}_{16}\text{H}_{36}\text{BrN}$) (capping agent), methylene blue dye ($\text{C}_{16}\text{H}_{18}\text{ClN}_3\text{S}$), ethanol ($\text{C}_2\text{H}_6\text{O}$), and ethylene glycol ($\text{C}_2\text{H}_6\text{O}_2$) all chemicals of analytical grades with high purity were used and which were purchased from Sigma Aldrich (St. Louis, MO, USA).

3.2. Preparation of Solutions

The stock solutions of 0.1 M $\text{Cu}(\text{CH}_3\text{COO})_2$, 0.1 M AgNO_3 , and 0.1 M TBAB were prepared in ethylene glycol using the standard solution preparation method [32], and the methylene blue dye solution was prepared in deionized water (extra pure, Charco chemicals).

3.3. Synthesis of Polyol-Mediated Ag–CuO NPs Using the Refluxing Method

Polyol-mediated Ag–CuO nanomaterial was synthesized using a simple refluxing method. During the synthesis, silver nitrate (AgNO_3) and copper acetate ($\text{Cu}(\text{CH}_3\text{COO})_2$) were used as sources of Ag and Cu, respectively, tetra butyl ammonium bromide (TBAB) was used as a capping agent, and ethylene glycol was used as a reducing agent. Stoichiometric amounts (5 wt.%) of silver nitrate, copper acetate, and TBAB were dissolved in ethylene glycol to form a suspension solution, and a 1:1 concentration ratio of the copper acetate and TBAB was used. The suspension solution was stirred for one hour ($60\text{ }^\circ\text{C}$) and added to the three-neck glass flask (Figure 9) with stirring and heated at 3 h ($90\text{ }^\circ\text{C}$) until a precipitate formed. The precipitate was filtered, washed with ethanol, and centrifuged 2–3 times. This precipitate was dried, grinded using mortar to form a powder, calcined at $550\text{ }^\circ\text{C}$ in the muffle furnace (3 h) after cooling to room temperature to obtain polyol-mediated Ag–CuO NPs and used for further characterization. In this study, only 5 wt.% silver nitrate-synthesized Ag–CuO nanomaterial characterization was mentioned due to its excellent results.

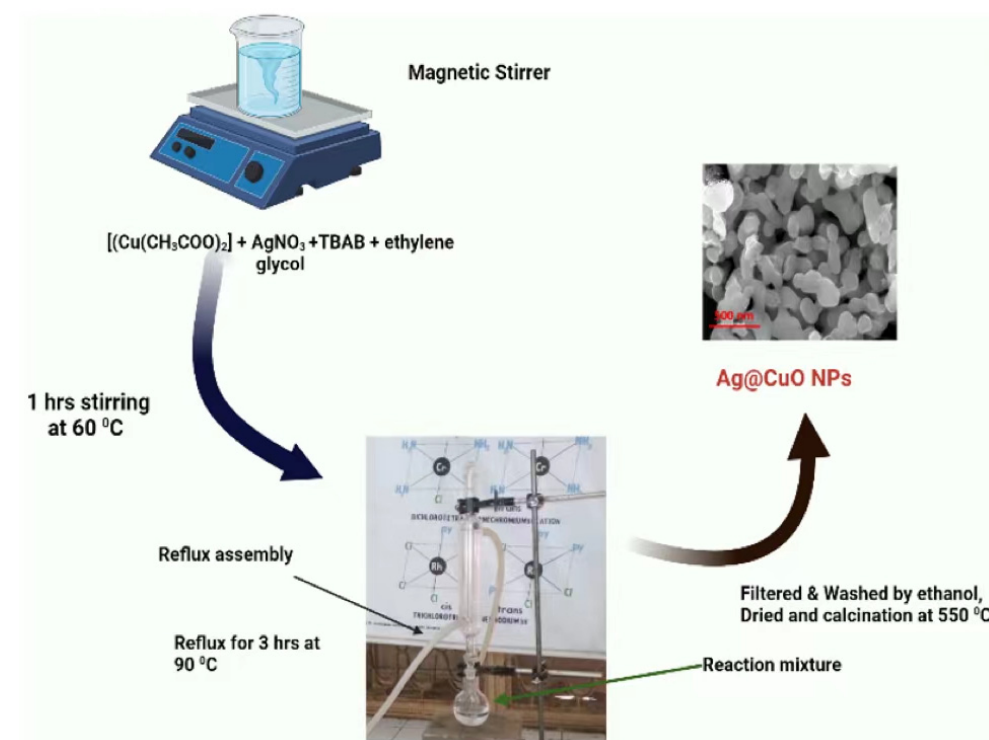
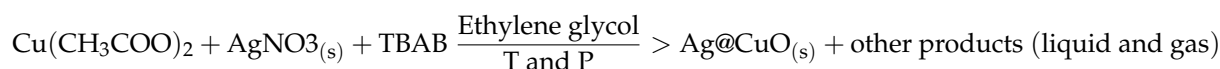


Figure 9. Synthesis of polyol-mediated Ag@CuO NPs.

The following may be the chemical reaction of polyol-mediated Ag@CuO NPs in ethylene glycol;



4. Conclusions

The synthesis of Ag@CuO nanomaterial was successfully achieved by incorporating 5 wt.% silver nitrates into copper oxide using the refluxing method in ethylene glycol solution with TBAB as the capping agent. XRD analysis revealed that the Ag@CuO NPs had an average particle size of 24.02 nm and a narrowed bandgap with an absorption edge shift from 200 to 300 nm towards a higher wavelength, indicating their potential for efficient photocatalysis. In comparison to other compounds, the polyol-mediated Ag@CuO NPs demonstrated the highest rate of methylene blue dye degradation of up to 94.43%. This efficient photocatalytic activity is attributed to the distinctive spherical structure and significant surface area of the Ag@CuO NPs, which facilitate effective charge transfer and inhibit e- and h+ pair recombination. The intensity of the UV-visible spectra obtained from the Ag@CuO NPs highlights their solid photocatalytic potential for future applications. Further research could focus on investigating the photocatalytic activity of these nanocomposites in various settings and exploring their potential in wastewater treatment and other environmental applications.

Author Contributions: Y.B., V.J., A.R., M.A. (Mohamed Abbas) and J.S.A. conceptualized, designed, and wrote the initial manuscript draft, S.A., M.A. (Mazen Almeahmadi), M.A. (Mamdouh Allahyani), D.V., K.K.Y., B.-H.J. and H.-K.P. prepared the figures and tables, and edited and revised the manuscript critically. H.-K.P. and B.-H.J. helped in funding acquisition. All authors have read and agreed to the published version of the manuscript.

Funding: The authors extend their appreciation to the Deanship of Scientific Research at King Khalid University (KKU) for funding this research through the Research Group Program under grant number R.G.P.2/517/44. The authors are thankful to the Deanship of Scientific Research at Najran University for funding this work, under Research Groups Funding program grant code NU/RG/SERC/12/45. This work was supported by the Mid-Career Researcher Program (grant no. 2020R1A2C3004237) through the National Research Foundation of the Republic of Korea.

Data Availability Statement: All data used to support the findings of this study are included in the article.

Conflicts of Interest: The authors declare no conflict of interest.

References

1. Soni, S.A.; Jadhav, V.R.; Kere, T.A. Effect of Copper Substitution, Calcination Temperature, and Photo-sensitizers on Photocatalytic Activity of Cu_{0.05}Zn_{0.95}O. *J. Chem. Environ. Sci. Appl.* **2018**, *5*, 1–9. [[CrossRef](#)]
2. Walunj, P.; Roy, A.; Jadhav, V.; Athare, P.; Dhaygude, A.; Aher, J.; Algethami, J.S.; Lokhande, D.; Alqahtani, M.S.; Bhagare, A.; et al. Polyol-mediated zinc oxide nanoparticles using the refluxing method as an efficient photocatalytic and antimicrobial agent. *Front. Bioeng. Biotechnol.* **2023**, *11*, 1177981. [[CrossRef](#)] [[PubMed](#)]
3. Chakraborty, S.; Kumar, R.; Nayak, J.; Jeon, B.H.; Dargar, S.K.; Tripathy, S.K.; Pal, P.; Ha, G.S.; Kim, K.H.; Jasiński, M. Green synthesis of MeOH derivatives through in situ catalytic transformations of captured CO₂ in a membrane integrated photo-microreactor system: A state-of-art review for carbon capture and utilization. *Renew. Sust. Energ. Rev.* **2023**, *182*, 113417. [[CrossRef](#)]
4. Kunwar, S.; Roy, A.; Bhusal, U.; Gacem, A.; Abdullah, M.M.; Sharma, P.; Yadav, K.K.; Rustagi, S.; Chatterjee, N.; Deshwal, V.K.; et al. Bio-Fabrication of Cu/Ag/Zn Nanoparticles and Their Antioxidant and Dye Degradation Activities. *Catalysts* **2023**, *13*, 891. [[CrossRef](#)]
5. Ardila-Leal, L.D.; Poutou-Piñales, R.A.; Pedroza-Rodríguez, A.M.; Quevedo-Hidalgo, B.E. A brief history of colour, the environmental impact of synthetic dyes and removal by using laccases. *Molecules* **2021**, *26*, 3813. [[CrossRef](#)] [[PubMed](#)]
6. Dikshith, T.S.S. *Hazardous Chemicals: Safety Management and Global Regulations*; CRC Press: Boca Raton, FL, USA, 2013.
7. Elgarahy, A.M.; Elwakeel, K.Z.; Mohammad, S.H.; Elshoubaky, G.A. A critical review of biosorption of dyes, heavy metals and metalloids from wastewater as an efficient and green process. *Clean. Eng. Technol.* **2021**, *4*, 100209. [[CrossRef](#)]

8. Gupta, V.K.; Ali, I.; Saleh, T.A.; Nayak, A.; Agarwal, S. Chemical treatment technologies for wastewater recycling—An overview. *Rsc. Adv.* **2012**, *2*, 6380–6388. [[CrossRef](#)]
9. Roy, A.; Elzaki, A.; Tirth, V.; Kajoak, S.; Osman, H.; Algahtani, A.; Islam, S.; Faizo, N.L.; Khandaker, M.U.; Islam, M.N.; et al. Biological synthesis of nanocatalysts and their applications. *Catalysts* **2021**, *11*, 1494. [[CrossRef](#)]
10. Raizada, P.; Sudhaik, A.; Patial, S.; Hasija, V.; Khan, A.A.P.; Singh, P.; Gautam, S.; Kaur, M.; Nguyen, V.H. Engineering nanostructures of CuO-based photocatalysts for water treatment: Current progress and future challenges. *Arab. J. Chem.* **2020**, *13*, 8424–8457. [[CrossRef](#)]
11. Ahmed, S.N.; Haider, W. Heterogeneous photocatalysis and its potential applications in water and wastewater treatment: A review. *Nanotechnology* **2018**, *29*, 342001. [[CrossRef](#)]
12. Ameta, R.; Solanki, M.S.; Benjamin, S.; Ameta, S.C. Photocatalysis. In *Advanced Oxidation Processes for Waste Water Treatment*; Academic Press: Cambridge, MA, USA, 2018; pp. 135–175.
13. Mani, V.M.; Kalaivani, S.; Sabarathinam, S.; Vasuki, M.; Soundari, A.J.P.G.; Das, M.A.; Elfakhany, A.; Pugazhendhi, A. Copper oxide nanoparticles synthesized from an endophytic fungus *Aspergillus terreus*: Bioactivity and anti-cancer evaluations. *Environ. Res.* **2021**, *201*, 111502. [[CrossRef](#)] [[PubMed](#)]
14. Shindhal, T.; Rakholiya, P.; Varjani, S.; Pandey, A.; Ngo, H.H.; Guo, W.; Ng, H.Y.; Taherzadeh, M.J. A critical review on advances in the practices and perspectives for the treatment of dye industry wastewater. *Bioengineered* **2021**, *12*, 70–87. [[CrossRef](#)] [[PubMed](#)]
15. Razali, M.; Kim, J.F.; Attfield, M.; Budd, P.M.; Drioli, E.; Lee, Y.M.; Szekely, G. Sustainable wastewater treatment and recycling in membrane manufacturing. *Green Chem.* **2015**, *17*, 5196–5205. [[CrossRef](#)]
16. Parvathiraja, C.; Shailajha, S. Bioproduction of CuO and Ag/CuO heterogeneous photocatalysis-photocatalytic dye degradation and biological activities. *Appl. Nanosci.* **2021**, *11*, 1411–1425. [[CrossRef](#)]
17. Chung, K.-H.; Kim, B.-J.; Park, Y.-K.; Kim, S.-C.; Jung, S.-C. Photocatalytic properties of amorphous N-doped TiO₂ photocatalyst under visible light irradiation. *Catalysts* **2021**, *11*, 1010. [[CrossRef](#)]
18. Cheriyaundath, S.; Vavilala, S.L. Nanotechnology-based wastewater treatment. *Water Environ. J.* **2021**, *35*, 123–132. [[CrossRef](#)]
19. Mittal, S.; Roy, A. Fungus and plant-mediated synthesis of metallic nanoparticles and their application in degradation of dyes. In *Photocatalytic Degradation of Dyes*; Elsevier: Amsterdam, The Netherlands, 2021; pp. 287–308.
20. Mondal, K.; Sharma, A. Recent advances in the synthesis and application of photocatalytic metal–metal oxide core–shell nanoparticles for environmental remediation and their recycling process. *RSC Adv.* **2016**, *6*, 83589–83612. [[CrossRef](#)]
21. Roy, A.; Sharma, A.; Yadav, S.; Jule, L.T.; Krishnaraj, R. Nanomaterials for remediation of environmental pollutants. *Bioinorg. Chem. Appl.* **2021**, *2021*, 1764647. [[CrossRef](#)]
22. Pawar, M.; Topcu Sendogdular, S.; Gouma, P. A brief overview of TiO₂ photocatalyst for organic dye remediation: Case study of reaction mechanisms involved in Ce-TiO₂ photocatalysts system. *J. Nanomater.* **2018**, *2018*, 5953609. [[CrossRef](#)]
23. Li, H.; Su, Z.; Hu, S.; Yan, Y. Free-standing and flexible Cu/Cu₂O/CuO heterojunction net: A novel material as cost-effective and easily recycled visible-light photocatalyst. *Appl. Catal. B Environ.* **2017**, *207*, 134–142. [[CrossRef](#)]
24. El Sayed, A.M.; Shaban, M. Structural, optical and photocatalytic properties of Fe and (Co, Fe) co-doped copper oxide spin coated films. *Spectrochim. Acta Part A Mol. Biomol. Spectrosc.* **2015**, *149*, 638–646. [[CrossRef](#)]
25. Maraj, M.; Raza, A.; Wang, X.; Chen, J.; Riaz, K.N.; Sun, W. Mo-doped CuO nanomaterial for photocatalytic degradation of water pollutants under visible light. *Catalysts* **2021**, *11*, 1198. [[CrossRef](#)]
26. Devi, L.V.; Sellaiyan, S.; Selvalakshmi, T.; Zhang, H.J.; Uedono, A.; Sivaji, K.; Sankar, S. Synthesis, defect characterization and photocatalytic degradation efficiency of Tb doped CuO nanoparticles. *Adv. Powder Technol.* **2017**, *28*, 3026–3038. [[CrossRef](#)]
27. Koffyberg, F.P.; Benko, F.A. A photoelectrochemical determination of the position of the conduction and valence band edges of p-type CuO. *J. Appl. Phys.* **1982**, *53*, 1173–1177. [[CrossRef](#)]
28. Roy, A.; Murthy, H.A.; Ahmed, H.M.; Islam, M.N.; Prasad, R. Phytogenic Synthesized of Metal/Metal Oxide Nanoparticles for Degradation of Dyes. *J. Renew. Mater.* **2022**, *10*, 1–20. [[CrossRef](#)]
29. Dasineh Khiavi, N.; Katal, R.; Kholghi Eshkalak, S.; Masudy-Panah, S.; Ramakrishna, S.; Jiangyong, H. Visible light driven heterojunction photocatalyst of CuO–Cu₂O thin films for photocatalytic degradation of organic pollutants. *Nanomaterials* **2019**, *9*, 1011. [[CrossRef](#)] [[PubMed](#)]
30. Kim, J.Y.; Hardy, J.S.; Scott Weil, K. Effects of CuO content on the wetting behavior and mechanical properties of a Ag–CuO braze for ceramic joining. *J. Am. Ceram. Soc.* **2005**, *88*, 2521–2527. [[CrossRef](#)]
31. Pitrubhakta, J.R.; Kere, T.A.; Shinde, S.S.; Soni, S.A.; Jadhav, V.R. Synthesis, Characterization, and Gas Sensing performance of Nanometer TiO₂ thick film by Hydrothermal method. *Asian J. Res. Chem.* **2020**, *13*, 360–364. [[CrossRef](#)]
32. Jadhav, V.R. Mathematical treatment to understanding the concentration terms. *Int. J. Res. Rev.* **2019**, *6*, 1–4.
33. Iqbal, S.; Javed, M.; Bahadur, A.; Qamar, M.A.; Ahmad, M.; Shoaib, M.; Raheel, M.; Ahmad, N.; Akbar, M.B.; Li, H. Controlled synthesis of Ag-doped CuO nanoparticles as a core with poly (acrylic acid) microgel shell for efficient removal of methylene blue under visible light. *J. Mater. Sci. Mater. Electron.* **2020**, *31*, 8423–8435. [[CrossRef](#)]
34. Bishnoi, S.; Kumar, A.; Selvaraj, R. Facile synthesis of magnetic iron oxide nanoparticles using inedible *Cynometra ramiflora* fruit extract waste and their photocatalytic degradation of methylene blue dye. *Mater. Res. Bull.* **2018**, *97*, 121–127. [[CrossRef](#)]
35. Ashraf, I.; Singh, N.B.; Agarwal, A. Green synthesis of iron oxide nanoparticles using Amla seed for methylene blue dye removal from water. *Mater. Today Proc.* **2023**, *72*, 311–316. [[CrossRef](#)]

36. Dasgupta, N.; Nayak, M.A.; Gauthier, M. Starch-Stabilized Iron Oxide Nanoparticles for the Photocatalytic Degradation of Methylene Blue. *Polysaccharides* **2022**, *3*, 655–670. [[CrossRef](#)]
37. Vanaja, M.; Paulkumar, K.; Baburaja, M.; Rajeshkumar, S.; Gnanajobitha, G.; Malarkodi, C.; Sivakavinesan, M.; Annadurai, G. Degradation of methylene blue using biologically synthesized silver nanoparticles. *Bioinorg. Chem. Appl.* **2014**, *2014*, 742346. [[CrossRef](#)] [[PubMed](#)]
38. Modi, S.; Yadav, V.K.; Gacem, A.; Ali, I.H.; Dave, D.; Khan, S.H.; Yadav, K.K.; Rather, S.-U.; Ahn, Y.; Son, C.T.; et al. Recent and emerging trends in remediation of methylene blue dye from wastewater by using zinc oxide nanoparticles. *Water* **2022**, *14*, 1749. [[CrossRef](#)]

Disclaimer/Publisher's Note: The statements, opinions and data contained in all publications are solely those of the individual author(s) and contributor(s) and not of MDPI and/or the editor(s). MDPI and/or the editor(s) disclaim responsibility for any injury to people or property resulting from any ideas, methods, instructions or products referred to in the content.